IL NUOVO CIMENTO Vol. 31 C, N. 1 Gennaio-Febbraio 2008
DOI 10.1393/ncc/i2008-10277-5

Charged particle effects: Experimental and theoretical studies on the mechanisms underlying the induction of molecular and cellular damage and the modulation of intercellular signalling

D. Alloni([1])([2]) and F. Antonelli([3])([4]), F. Ballarini([1])([5]), M. Belli([3])([4]), A. Bertolotti([1])([5]), A. Campa([3])([4]), V. Dini([3])([4]), L. D'Ercole([6]), G. Esposito([3])([4]), A. Facoetti([1])([5]), W. Friedland([7]), C. Giovannini([3]), S. Grande([3])([4]), L. Guidoni([3])([4]), M. Liotta([5])([9]), F. Lisciandro([6]), A. M. Luciani([3])([4]), L. Mantovani([6]), L. Mariotti([1])([5]), S. Molinelli([10]), R. Nano([5])([8]), A. Ottolenghi([1])([5])(*), A. Palma([3]), H. G. Paretzke([7]), F. Pasi([5])([8]), L. Raffaele([11]), A. Rosi([3])([4]), O. Sapora([12])([4]), D. Scannicchio([1])([5]), G. Simone([3])([4]), E. Sorrentino([3])([4]), M. A. Tabocchini([3])([4]) and V. Viti([3])([4])

([1]) *Dipartimento di Fisica Nucleare e Teorica, Università di Pavia - via Bassi 6 27100 Pavia, Italy*
([2]) *LENA (Laboratorio di Energia Nucleare Applicata), Università di Pavia - via Bassi 6 27100 Pavia, Italy*
([3]) *Dipartimento di Tecnologie e Salute, Istituto Superiore di Sanità - Viale Regina Elena 299 00161 Rome, Italy*
([4]) *INFN, Sezione di Roma, Gruppo Collegato Sanità - Viale Regina Elena 299 00161 Rome, Italy*
([5]) *INFN, Sezione di Pavia - via Bassi 6, 27100 Pavia, Italy*
([6]) *Struttura Complessa di Fisica Sanitaria, Fondazione Policlinico San Matteo IRCCS 27100 Pavia, Italy*
([7]) *Institute of Radiation Protection, Helmholtz Zentrum München - Ingolstädter Neuherberg, Germany*
([8]) *Dipartimento di Biologia Animale, Università di Pavia - 27100 Pavia, Italy*
([9]) *Dipartimento di Fisica, Università di Milano - via Celoria 16, 20133 Milano, Italy*
([10]) *Fondazione CNAO - via Caminadella 16, 20123 Milano*
([11]) *INFN, Laboratori Nazionali del Sud - Catania, Italy*
([12]) *Dipartimento Ambiente e Connessa Prevenzione Primaria, Istituto Superiore di Sanità Viale Regina Elena 299, 00161 Rome, Italy*

(ricevuto l' 11 Giugno 2008; pubblicato online il 16 Settembre 2008)

Summary. — In this paper we present the main outcomes of a wide collaborative effort (carried out within the INFN project "EPICA" and in part within the European projects "RISC-RAD" and "NOTE" and the ASI project MoMa-COUNT),

(*) E-mail: andrea.ottolenghi@pv.infn.it

both experimental and theoretical, devoted to the characterization and quantification of the induction of DNA-targeted and non-DNA-targeted molecular and cellular biological endpoints, following irradiation of human cells with different charged particles. The work was mainly aimed at reaching a better understanding of the mechanisms governing the physical and biophysical pathways leading from the initial energy deposition by radiation in matter to the induction of observable radiobiological damage, with particular focus on the role played by radiation quality. More specifically, we characterized the induction of DNA DSB within different fragment-size ranges outlining the effectiveness of high-LET radiation at inducing small fragments and thus clustered DNA breaks, which can evolve in terms of endpoints like chromosome aberrations (CAs). This was confirmed by the development and application of a model of CA induction based on the assumption that only clustered DNA breaks can lead to aberrations. Concerning non-DNA-targeted damage, we quantified the time-dependent induction of medium-mediated DNA damage in bystander cells and we characterized the time and dose dependence of cytokine concentration in the culture medium of sham-irradiated and irradiated cells, since medium-mediated bystander damage is thought to arise from molecular signalling between irradiated and unirradiated cells. The mechanisms governing such signalling were investigated developing a model and a MC code simulating cytokine release, diffusion and internalization, showing good agreement with experimental data. Non-DNA-targeted effects were further characterized by MRS investigation of the radiation effects on lipids and oxidative metabolism, which are particularly relevant also considering that they may be differently expressed in different tumors and in normal tissues.

PACS 87.53.-j – Effects of ionizing radiation on biological systems.

1. – Introduction

The mechanisms driving the *ensemble* of events leading from the initial energy deposition by radiation to the production of lesions to the DNA and other biological molecules and to the processing of such lesions in terms of biological endpoints at different levels (*e.g.*, DNA and chromosome damage, damage to the cell membranes and the cell metabolisms, cell death, etc.) are still not known in detail. In particular, further studies are desirable to clarify the role played by radiation quality (*i.e.* particle type and energy), which in turn is largely determined by radiation track structure. Indeed, the spatial distribution of the excitations and ionizations occurring in the target atoms and molecules is a crucial issue for determining the induction of DNA damage clusters, which play a fundamental role for the subsequent evolution of the initial radiation insult in terms of radiobiological endpoints at molecular, cellular and multi-cellular level. Reaching a better understanding on the action of charged particles such as protons, He ions and heavier ions like carbon, is of fundamental importance in the field of hadron therapy, which is based on the dose localization in the Bragg peak region and, for carbon ions, on the higher relative biological effectiveness (RBE) of these particles.

Also the consequences of irradiation on cellular communication urgently need further investigation, especially considering that possible alterations in the cellular communication pathways can lead to the induction of the so-called "bystander effects". The latter consist in the induction of damage in cells which have not been traversed by radiation, but have received molecular signals by irradiated cells. Phenomena like bystander effects,

which have been observed for different endpoints and with different approaches, can have significant implications both for radiotherapy and for radiation protection. In particular, the non-linearity observed for some dose-response curves at low doses may affect the radiation risk assessment at low doses, which is currently based on the so-called "Linear-No-Threshold hypothesis", based on linear, no-threshold back-extrapolations from epidemiological data at higher doses. A large amount of data on bystander effect has been accumulated in the last decade. However, the knowledge about the underlying mechanisms remains poor. It is now widely accepted that such effects are due to cellular communication, not only via gap-junctions (*i.e.* small channels directly connecting the cytoplasms of adjacent cells allowing diffusion of ions and molecules smaller than 2000 Dalton) but also via release of Reactive Oxygen Species (ROS, such as H_2O_2 and O_2^-), Nitric Oxyde (NO) and larger molecules (typically cytokines), as well as more complex structures like vesicles. The effects on the cell membranes, which can be classified as "non-DNA-targeted effect" in the sense that the double helix is not the main target, can play an important role as well. Also, depending on the specific characteristics of the irradiated target (*e.g.*, cell type, cell-cycle stage, etc.), it is likely that different signals are involved. A typical example of a possible pathway consists of *intra*cellular communication via production of ROS in the irradiated cell, followed by *inter*cellular communication through diffusion of small molecules in the gap junctions and/or larger molecules (typically cytokines) in the extracellular environment, which in turn can be internalized by the membrane receptors of unirradiated cells thus triggering a cascade of signalling events leading to molecular and/or cellular damage in unirradiated cells.

In this context, within the INFN project "EPICA" we investigated experimentally and theoretically the induction of both "DNA-targeted" effects (such as DNA and chromosome damage) and "non-DNA-targeted" effects (such as membrane damage, bystander effect and cell communication). Particular attention was devoted to the dependence of these effects on radiation quality, since it is well known that the energy deposition pattern strongly modulates the features of the initial damage and thus its reparability. More specifically, we investigated the induction of DNA double-strand breaks (DSB), chromosome aberrations and cell death following irradiation with light and heavy charged particles as well as with gamma-rays, which were taken as reference radiation. In parallel, we investigated the time-dependent release, diffusion and internalization of specific cytokines, which are candidate signals in bystander effect phenomena, and the induction of damage in important non-DNA target such as lipids and oxidative metabolism.

2. – DNA-targeted-effects

2˙1. *DNA damage: experimental studies.* – It is widely accepted that DNA double-strand breaks are critical lesions in the pathways leading from the initial energy deposition by radiation to radiobiological damage at sub-cellular and cellular level, including gene mutations, chromosome aberrations, neoplastic transformation and clonogenic inactivation. The spatial distribution of the initial DSB plays a key role in determining the fate of irradiated cells, since the sub-cellular and cellular endpoints mentioned above do depend on the features of the DSB ensemble induced by the irradiation [1]. The spatial correlation of DSB, both in terms of geometrical distance and in terms of "genomic distance" (*i.e.* in base-pairs), is thought to influence the DSB reparability. This may explain why the radiobiological effects induced by a given radiation dose depend on the radiation quality, since the DSB distribution will be determined not only by chromatin conformation, but also by radiation track-structure at the nanometre level. Experimental and

theoretical studies (*e.g.*, [2-4]) outlined the existing correlation of radiation-induced DSB at the nucleosome scale (*i.e.* $\approx$ 100 base-pairs or bp), and at the low-level chromatin fibre organization scale (*i.e.* $\approx$ 1 kbp). For high-LET radiation, including heavy ions, such correlation is much higher than for low-LET radiation. Even at larger scales, where the distribution of the DSB induced by low-LET radiation is basically random, high-LET radiation can produce a DSB distribution that deviates significantly from randomness (*e.g.*, [5,6]). The statistical properties of the induced DSB can be investigated analysing the DNA fragment size distributions produced after irradiation. The analysis of DNA fragment spectra can provide an important basis for developing models able to reliably predict the consequences of high-LET irradiation.

DNA fragmentation by high doses of heavy ions was studied in the fragment-size range 1–5700 kbp, following irradiation of AG1522 primary human fibroblasts, embedded in agarose plugs, with iron ion beams of various energies at different radiobiological facilities, namely at the Heavy Ion Medical Accelerator (HIMAC) of the National Institute of Radiological Sciences (NIRS) in Chiba, Japan (500 and 200 MeV/u iron beams) and at the Alternating Gradient Synchrotron (AGS) and the NASA Science Research Laboratory (NSRL) accelerators of the Brookhaven National Laboratory (BNL) in Upton, USA (5 and 1 GeV/u iron beams). Gamma-rays from the ^{60}Co source at the Istituto Superiore di Sanità (ISS) in Rome, Italy, were used as reference radiation. In order to avoid DSB repair during irradiation, the plugs were kept at 0–4 °C. The dose rate was 10–15 Gy min^{-1} and the dose range was 40–200 Gy for all the considered radiation types. After irradiation, the plugs were incubated in lysis solution, then washed and stored at 4 °C until processed. DNA damage was evaluated by calibrated Pulsed-Field Gel Electrophoresis (PFGE) and Constant-Field Gel Electrophoresis (CFGE) using different electrophoretic conditions to measure the number of fragments in the following ranges: 1–9 kbp, 9–23 kbp, 23–1000 kbp and 1000–5700 kbp [7]. The analysis of the fragmentation spectra showed that the correlation of DSB positions, absent in the case of gamma-ray irradiation, increases markedly with LET for the iron-ion beams. DSB correlation was shown to be dose dependent, decreasing when the dose increases. This can be explained considering that with increasing dose there is an increasing fraction of DNA fragments produced by DSB due to different, uncorrelated tracks [7, 8].

In order to investigate radiation-induced DNA damage and repair at low doses, immunofluorescence techniques have recently been developed based on antibodies against proteins involved in DNA damage response. In particular, detection of phosphorylation of the variant histone H2AX (γ-H2AX) has provided a valuable and highly sensitive method to monitor DSB formation. The assay is based on the evidence that, rapidly after irradiation, many molecules of histone H2AX become phosphorylated along Mega-base chromatin domains adjacent to a DSB [9]. Using fluorescent antibodies, such lesions can be visualized as foci (see fig. 1) and their enumeration at different times from irradiation can be used to measure DSB induction and processing. This technique is at present the only one which allows investigation of DNA damage and repair in single cells at doses as low as those released by one particle traversal. Moreover, foci persistence has been suggested as a potential predictor of cell radiation sensitivity [10].

With this assay we investigated the time course of DBS induction and processing after irradiation of AG1522 primary human fibroblasts with 0.5 Gy gamma-rays, carbon ions and alpha-particles. Parallel experiments were performed to evaluate cell killing and lethal mutations (early and late survival). Irradiation with 62 MeV/u carbon ions (LET = 40 keV/μm) was performed at the superconductive cyclotron of INFN-Laboratori Nazionali del Sud in Catania, Italy, whereas irradiations with alpha-particles from Am-241

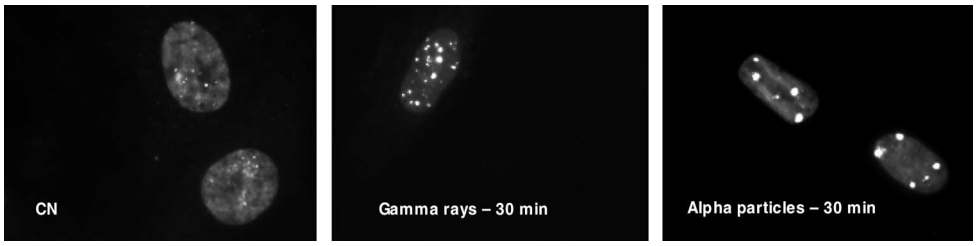

Fig. 1. – *In situ* immunofluorescence detection of γ-H2AX foci in AG1522 cells 30 minutes after irradiation with gamma-rays or alpha-particles. Control cells are also shown in the left panel.

(LET = 125 keV/μm) and with gamma-rays from Cs-137 were both performed at the ISS in Rome, Italy. Figure 2 compares the results obtained for DSB induction and processing. In all cases, the maximum number of foci was obtained at 30 minutes after irradiation and represents the initially induced damage. The finding that this is higher for gamma-rays than for charged particles can be explained considering that C-ions and alpha-particles are densely ionizing and induce DSB which are spatially correlated at distances that cannot be resolved as individual foci. This also means that the γ-H2AX assay may underestimate the number of DSB induced by densely ionizing radiation. However, it is interesting that the maximum number of foci is consistent with the number of tracks producing at least 1 DSB. Moreover, at longer times after irradiation the decrease in the foci number is smaller for charged particles than for gamma-rays, the foci observed after irradiation with alpha-particles being more persistent. This finding may be partly related to the presence of multiple foci along the same track, but also suggests the presence, within the same focus, of multiple and/or complex DSB, which are more difficult to be repaired with respect to gamma-ray–induced DSB. This is consistent with the higher biological effectiveness of charged particles at inducing cellular effects, as revealed by the results we obtained for cell killing (data not shown).

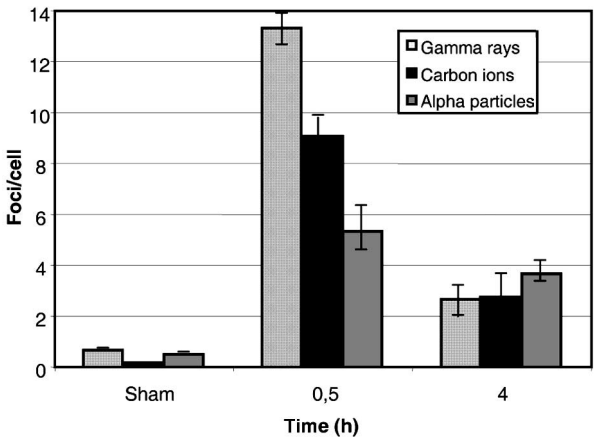

Fig. 2. – Number of foci per cell induced by gamma-rays, carbon ions or alpha-particles 30 minutes or 4 hours after irradiation.

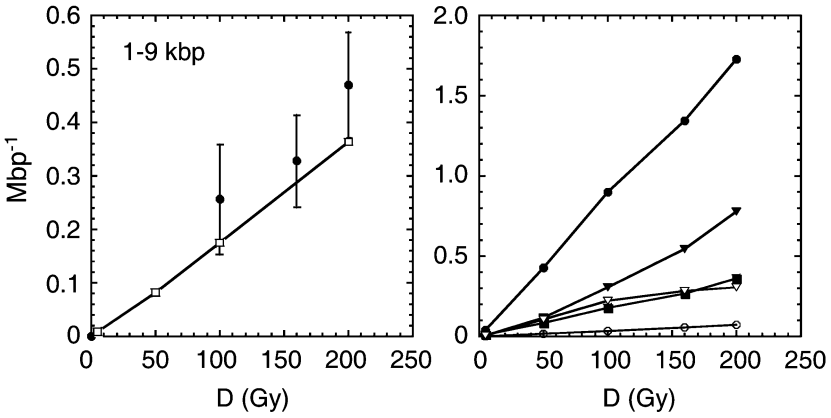

Fig. 3. – Number of DNA fragments per Mbp induced by 115 MeV/u iron ions, as a function of dose. Left panel: experimental data (full symbols) with error bars and PARTRAC simulation data (open symbols, linked by a line as a guide for the eye) at the following dose values: 5 Gy, 50 Gy, 100 Gy, 150 Gy and 200 Gy, for fragments in the size range 1–9 kbp. Right panel: PARTRAC simulation data (linked by lines as guides for the eye) at the same doses. The different symbols in the right panel refer to different fragment size ranges: 0–1 kbp (full circles), 1–9 kbp (full squares), 9–23 kbp (open circles), 23–1000 kbp (full triangles), 1000–5700 kbp (open triangles).

2˙2. *DNA damage: phenomenological and mechanistic models of DNA fragmentation.* – In this subsection we report a theoretical analysis, both mechanistic and phenomenological, of DNA fragmentation induced by iron ions. A similar study on alpha-particles has been described elsewhere [11]. For both iron ions and alpha-particles, the mechanistic analysis was performed by means of the PARTRAC code, which is a biophysical Monte Carlo code (mainly developed at the GSF Institute in Munich, Germany) based on an "event-by-event" description of radiation track structure in liquid water at the nm level, combined with an atom-by-atom description of a DNA target model representing the whole genome (6 Gbp) of a diploid human fibroblast in interphase. The simulated target presents six levels of DNA organization (deoxynucleotide pair, double helix, nucleosome, chromatin fibre, chromatin fibre loops and chromosome territories). The current version of PARTRAC can simulate the transport and interaction of electrons, photons, protons, helium ions and heavier ions. Further details can be found elsewhere [12]. In the study presented herein, a model cell lying on a mylar base was irradiated from the bottom with a beam. Each energy deposition event in the cell nucleus was recorded; starting points, energy and directions of secondary electrons were used as input data of the electron module. The simulated yields of radiation-induced DNA strand breaks were determined by superposition of the inelastic event track-structure pattern on the DNA target model. The probability of inelastic energy deposition events in that volume producing a SSB was assumed to be 0 for energy depositions smaller than 5 eV, to increase linearly from 0 to 1 for energy depositions in the range 5–40 eV, and to be equal to 1 for energy depositions larger than 40 eV. The effects of OH-radical attack were taken into account as well. A DSB was assumed to occur when two SSB were found on opposite strands within 10 bp.

Figure 3 reports experimental and calculated yields of DNA fragments (per Mbp) of different sizes (1–9 kbp for the experiments; 0–1 kbp, 1–9 kbp, 9–23 kbp, 23–1000 kbp,

1000–5700 kbp for the PARTRAC simulations) induced by 115 MeV/u Fe ions. The agreement between experiments and simulations can be considered satisfactory, given that no *a posteriori* adjustment of the code parameters was introduced. This gives confidence on the results obtained with PARTRAC, which was also applied to the simulation of DNA fragments smaller than 1 kbp and larger than 5700 kbp. Importantly, fragments smaller than 1 kbp account for about half of the total fragments, leading to a higher RBE value with respect to the fragments of any size. This reflects the features of radiation track-structure, which for high-LET radiation—including heavy ions—is particularly effective at producing clustered energy depositions and thus very small DNA fragments. Even though the experimental detection of such fragments is not easy, they can play an important role in the evolution of the initial DNA damage in terms of subsequent endpoints at sub-cellular and cellular level, because clustered DNA breaks are more difficult to be repaired correctly and thus can give rise to gene mutations, chromosome aberrations, etc. In this context, in the next section we will present a theoretical model based on the assumption that only clustered—and thus severe—DNA breaks can give rise to chromosome aberrations.

The phenomenological analysis, aimed at evaluating the DSB spatial correlation on the basis of the departure of their distribution from randomness, was performed by means of the Generalized Broken Stick (GBS) model, which has been introduced and described in detail in previous works [13]. The GBS model was developed with the purpose of analyzing the DSB spectrum, taking into account that not all the DSB revealed by electrophoresis are induced by radiation. In the genome there are always endogenous breaks, and others are also caused by the experimental procedures. The relevant issue is how the model can provide, starting from the experimental data, parameters related to the DSB spatial correlation. The main quantity is the DSB yield, *i.e.* the number of radiation-induced DSB per unit dose and unit DNA mass. The three following fragment-size ranges were chosen: 1–9 kbp (small fragments), 145–750 kbp (intermediate fragments) and 750–2700 kbp (large fragments). The number of fragments in each of the three ranges, and for each experimental dose value, was computed, leaving the yield as a free parameter of the model. By fitting the computed number of fragments to the measured one, for each size range and for each dose, three dose-dependent yields were obtained (denoted by y_1, y_2 and y_3), corresponding to the three ranges 1–9 kbp, 145–750 kbp and 750–2700 kbp, respectively.

To evaluate the departure from randomness of the experimental DSB distribution, we compared the DSB yields in these three fragment size regions (y_1, y_2 and y_3) by means of two parameters, *i.e.* the ratios $R_\mathrm{s} = y_1/y_3$ and $R_\mathrm{m} = y_2/y_3$. If random breakage occurs, R_s and R_m are equal to unity at all doses, within the experimental errors. On the contrary, a significant difference from unity would indicate a DSB correlation. These parameters were analyzed both as a function of LET, *i.e.* with respect to different radiation qualities, and as a function of dose for any given radiation.

Figure 4 shows the R_s and R_m values for the beam with the highest LET analyzed so far, *i.e.* 115 MeV/u iron ions. Both R_s and R_m are higher than unity at all doses.

2˙3. *Chromosome damage: a model of chromosome aberration induction.* – Despite the recent significant advances in the experimental techniques and the large amount of available experimental data, some aspects of the mechanisms governing the induction of chromosome aberrations have not yet been fully elucidated. For instance, it is still not clear whether any DNA double-strand break, independently of its complexity, can participate the formation of chromosome aberrations, or if only clustered—and thus severe—breaks

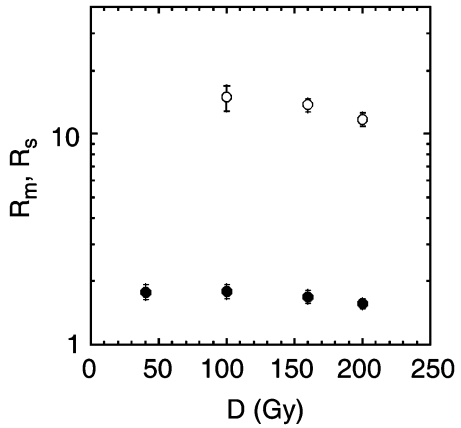

Fig. 4. – Parameters $R_{\rm m}$ (full symbols) and $R_{\rm s}$ (open symbols), in semi-log scale, as a function of dose for DNA fragmentation induced in human fibroblasts by 115 MeV/u iron ions.

are involved. Furthermore, the dependence of the interaction probability between two chromosome breaks on their distance is still a matter of debate. Theoretical models and simulation codes can be of great help both for interpreting experimental observations and for performing extrapolations where experimental data are not available, typically at low doses and/or low dose rates. Various modelling approaches can be found in the literature, and many of them are based on Lea's "Breakage-and-Reunion" theory [14]. According to Lea, the radiation can induce chromosome breaks, and each break produces two independent chromosome free ends. Those free ends that are sufficiently close do interact and give rise to exchange-type aberrations via pair-wise "mis-rejoining". In 1999 we initiated the development of an *ab initio* mechanistic model and a Monte Carlo code based on radiation track structure at the nanometre level [15]. The current version of the model can simulate the induction of the main chromosome aberration types (including dicentrics, translocations, rings, various complex exchanges and deletions) in human cells exposed to photons, light ions—typically protons and alpha-particles—and now also heavy ions such as carbon and iron [16-20]. The main assumption of the model consists of regarding chromosome aberrations as the "evolution" of clustered DNA breaks, which are called "Complex Lesions" (CLs). Each CL is assumed to produce two independent chromosome free ends, and only free ends induced in neighbouring chromosomes or in the same chromosome are allowed to join and give rise to exchange-type aberrations. The current version of the model mainly deals with human lymphocyte nuclei, which are modelled as 3-μm-radius spheres. The implementation of human fibroblast nuclei is in progress. For both lymphocytes and fibroblasts, the 46 interphase chromosome territories are described as (irregular) intra-nuclear domains with volume proportional to the chromosome DNA content, and each territory consists of the union of small adjacent cubic boxes. For a given radiation quality (*i.e.* particle type and energy), the yield of induced CL·Gy^{-1}·cell^{-1}, taken from track-structure simulations provided by the PARTRAC code mentioned above, is the starting point for dose-response simulations. While for photons the lesions are randomly distributed in the cell nucleus, for light ions they are located along straight lines representing the cell nucleus traversals. Concerning heavy ions, a fraction of the lesions induced by a heavy ion are "shifted" radially with

TABLE I. – *Predicted and observed whole-genome Simple Exchanges (dicentrics plus reciprocal translocations) per* 100 *cells induced in human lymphocytes exposed to different doses of* 147 *keV/μm Fe ions (nominal energy:* 1 *GeV/n). The experimental data reported for comparison were taken from* [21].

Dose (Gy)	Model prediction	Exp. data
0.2	13.2	16.6 ± 2.5
0.5	31.1	46.5 ± 6.0
1.0	64.4	76.3 ± 12.9
1.5	94.4	94.5 ± 18.2
2.0	115.6	114.3 ± 19.9

respect to the primary-ion track to take into account the delta-ray effects. Specific background (*i.e.* prior to irradiation) yields for different aberration types can be included. Both Giemsa staining and whole-chromosome FISH painting can be simulated, and the implementation of multi-FISH is in progress. The code provides dose-response curves for the main aberration types, directly comparable with experimental data. Until now, the model has been tested for gamma-rays, protons and helium ions. The good agreement between model predictions and experimental data allowed for model validation, especially considering that no *a posteriori* fit was performed [15-19]. The extension of the model to heavy ions has started only recently, and the results are still preliminary. Dose-response curves for the induction of different chromosome aberrations by gamma-rays and light ions can be found in previous publications. Table I reports whole-genome Simple Exchanges (*i.e.* dicentrics plus reciprocal translocations) per 100 cells induced in human lymphocytes exposed to different doses of 147 keV/μm Fe ions (nominal energy: 1 GeV/n). Literature-based experimental data [21] obtained with the same particle type, energy and dose (and with the same cell type) are also reported for comparison. The agreement between simulations and data strengthens the model, and hence the assumption that clustered DNA breaks play a fundamental role in the evolution of DNA damage in terms of chromosome aberrations and possibly other radiobiological endpoints such as gene mutations, cell death and cell conversion to malignancy. It is also worth mentioning that the model has been applied to the evaluation of the induction of Chronic Myeloid Leukaemia [17], which is thought to arise from a reciprocal translocation between chromosomes 9 and 22, and to the estimate of aberration yields observed in astronauts' lymphocytes following long-term missions onboard the Mir space station and the International Space Station [18].

3. – Non-DNA-targeted effects

3˙1. *Molecular and cellular damage in bystander cells.* – DNA damage in bystander cells can be studied by using the H2AX assay-to visualize DSB induced in unirradiated cells grown in co-culture with directly irradiated cells. In this work, bystander cells were grown on the surface of a permeable porous membrane which represents the bottom of transwell inserts. The pores allow the passage of signalling molecules possibly released by cells directly irradiated with 0.5 Gy alpha-particles (dose rate of about 0.08 Gy/min) at 37 °C. Bystander cells were kept in co-culture with irradiated cells for 30 minutes, 1 hour or 2 hours. After that, these cells were fixed and DSB were visualized as γ-H2AX foci using the fluorescent technique described in subsect. **2**˙1. Figure 5 shows the percentage

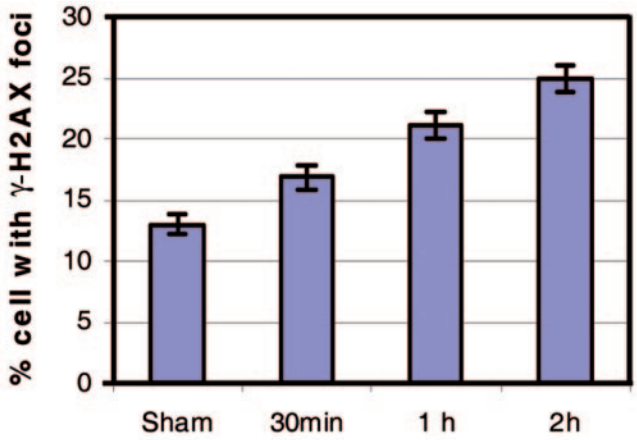

Fig. 5. – Effect of the time of co-culturing of targeted and bystander cells on the induction of γ-H2AX foci in bystander cells. Targeted cells were irradiated with 0.5 Gy alpha-particles.

of bystander cells with γ-H2AX foci after 30 minutes, 1 hour and 2 hours of co-culture with irradiated cells. A slight increase in the number of positive cells with respect to the sham control is visible at 30 min of co-culture, which becomes more evident after 1 and 2 hours of co-culture. In this system, in which targeted and bystander cells are not in contact, communication between irradiated and unirradiated cells by gap-junctions is prevented, so that only the effect of signalling molecules released in the culture medium has to be considered (*i.e.* the so-called "medium-mediated bystander effect"). These results clearly show a response in terms of DNA damage in bystander cells and, although gap-junctions play an important role in the induction of non-targeted effects [22], even in the absence of such type of communication a bystander effect is still evident. The degree of this response seems to increase, under the conditions considered herein, with the co-culture time.

3˙2. *Cytokine release and its modulation by radiation: experimental and theoretical studies.* – Cytokines are considered to be one of the best groups of molecules candidate for the transmission of the wide variety of bystander effects observed so far. Nevertheless, there are discordant reports of decreased/increased expression or no change in expression of some of these molecules after radiation exposure. This may reflect the well-known dependence of cytokines on cell or tissue type and pre-existing pathways or conditions for their expression. For these reasons, the first approach we used to the study of the cytokines involved in the transmission of bystander effects, was to screen the simultaneous modulation of a panel of 18 different cytokines after the exposure to gamma-rays (Cobalt-60 at the Fondazione Policlinico San Matteo, Pavia) and alpha-particles (from the Am-241 source at the ISS, Rome) by means of the chemiarray technique (Human Cytokine Set 1 Cartesian Array, Biosource).

A comparison between chemiarray profiles of culture media collected and filtered after gamma-rays and alpha-particles exposure did not show any cytokine produced *ex novo* or inhibited after ionising radiation exposure. However, some appreciable differences in the signal intensity were observed for IL-6, IL-8 and IL-12 in samples collected 20 hours after irradiation from both glioblastoma cells (T98G) and fibroblasts (AG1522) (fig. 6).

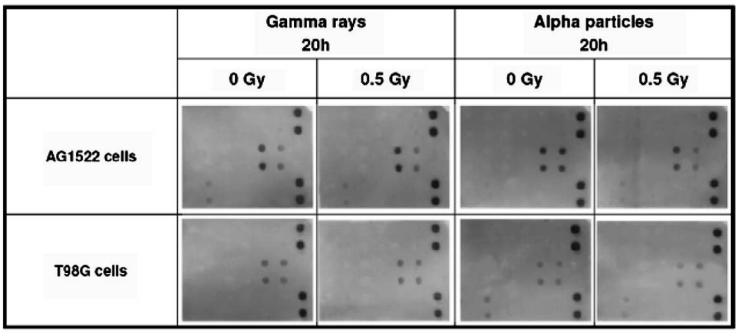

Human Cytokine Set 1 Cartesian Array™ Map

	a	b	c	d	e	f	g
1	Eotaxin	GM-CSF	IP-10	TNF-α	RANTES	Leptin	Pos* (***)
2	Eotaxin	GM-CSF	IP-10	TNF-α	RANTES	Leptin	Pos*
3	IL-1α	IL-1β	IL-3	IL-4	IL-6	IL-8	Neg**
4	IL-1α	IL-1β	IL-3	IL-4	IL-6	IL-8	Neg**
5	IL-10	IL-12	IL-17	MIP-1α	MIP-1β	MIP-5	Pos*
6	IL-10	IL-12	IL-17	MIP-1α	MIP-1β	MIP-5	Pos*

* Positive Control Wells
** Negative Control Wells

Fig. 6. – Chemiarray profiles of medium samples collected from human fibroblasts (AG1522) and human glioblastoma cells (T98G) 20 hours after exposure to gamma-rays and alpha-particles. Lower panel: human Cytokine Set 1 Cartesian Array map.

Subsequently, to quantify the differences observed with chemiarrays, we evaluated the modulation of IL-6 and IL-8 over a time interval of 22 hours after different doses (0.25, 0.5 and 1 Gy) of alpha and gamma irradiation in comparison with sham irradiation by means of ELISA. Figure 7 illustrates the data concerning IL-6 concentrations after exposure of AG1522 cells to gamma-rays.

Interestingly, gamma irradiation determined alterations of IL-6 release into the medium that were not linearly correlated to the dose: at 20 hours, a dose of 0.25 Gy determined a significant increase of IL-6 compared to sham irradiation, however 0.5 Gy and 1 Gy caused a decrease in the concentration of this cytokine into the medium. The same trend was observed at 5, 7 and 8 hours after exposure.

Exposure to the same doses of carbon ions affected IL-6 release at earlier times: within 5 hours it was possible to detect increased concentrations with a linear dose dependence relationship (data not shown).

3˙3. *Cytokine receptor expression in irradiated and bystander cells.* – The cell-specificity in the induction of bystander effects and the cell-specificity to receive the secreted signals that have been described so far clearly suggest that both the ability of producing cytokines as well as the receptor profiles are likely to determine the cell's responses and the final endpoint. Indeed, at cellular level, the flow of information is initiated by the interaction of a ligand (*i.e.* cytokine) with an activated membrane receptor which transmits the signal from the outside to the inside of a cell where a cascade of events is initiated.

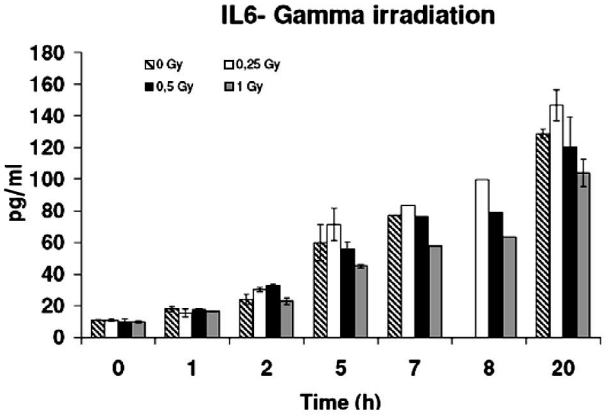

Fig. 7. – Time-dependent concentration in the medium of IL-6 in AG1522 cells after sham irradiation (0 Gy) 0.25 Gy, 0.5 Gy and 1 Gy. 5000 cells/cm^2 were seeded 20 hours prior irradiation. Values are presented as means of duplicate samples from three independent experiments.

We qualitatively evaluated by immunocytochemistry the receptor profiles of IL-6, IL-8 and TGFβ in gamma-irradiated AG1522 and T98G cells fixed 20 hours after exposure and whose medium was collected, filtered and transferred to unirradiated cells for 20 hours. In fig. 8 some representative patterns for TGFβ receptor expression in irradiated and bystander cells are shown. The immunostaining for this growth factor in AG1522 cells irradiated with a dose of 0.5 Gy showed that this dose causes an increase of its expression. However, incubation for 20 hours in medium collected from these irradiated cells determined a similar increase on the receptor expression in non-irradiated cells. Concerning T98G cells, the directly irradiated cells exhibited a more pronounced increase of the receptor expression, whereas the effect observed in bystander cells after the treatment with conditioned medium was similar to that observed in fibroblasts.

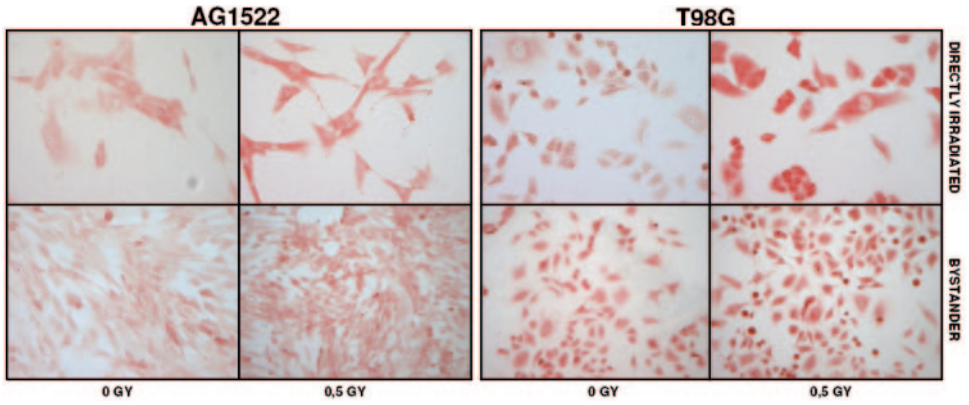

Fig. 8. – Representative immunocytochemistry staining for TGFβ receptor in AG1522 e T98G cells. Upper pictures: directly irradiated cells 20 hours after irradiation with 0.5 Gy gamma-rays in comparison with sham-irradiated cells. Lower pictures: bystander cells incubated for 20 hours with medium harvested from irradiated cells and sham-irradiated cells.

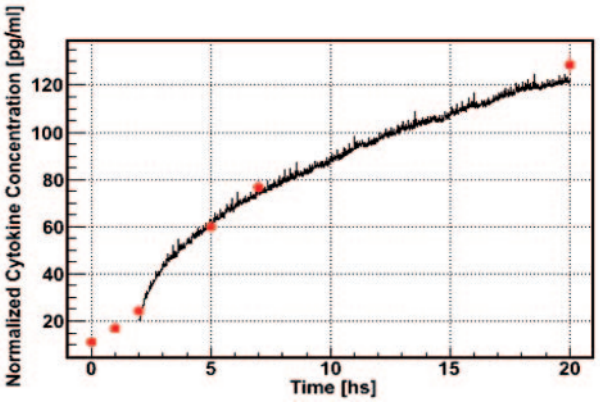

Fig. 9. – Monte Carlo simulations (line) and experimental measurements (full circles) of the IL-6 present in the culture medium of 250000 "sham irradiated" fibroblasts.

Investigations are still needed on the quantification of the production rate and of the mechanisms regulating the transmission of the signals, such as depletion (*i.e.* internalization of signalling molecules by cells via specific membrane receptors) and degradation (*i.e.* removal of signalling molecules due to interaction with enzymes—typically proteases—that degrade the "original" molecules).

In order to address these questions, we developed a model and a Monte Carlo code to simulate the time-dependent regulation of IL-6 in the case of 250000 "sham irradiated" fibroblasts. On first approximation, we simulated a geometry that follows the experimental set-up (properly re-scaled), and each cell is assumed to release cytokines with a constant rate left as a free parameter. The molecules, once released from cells, are "transported" by means of diffusion based on a Brownian-motion model, with a root mean square displacement of $\sqrt{6Dt}$. The value of the diffusion coefficient D was fixed at $10^8\,\mathrm{nm}^2/\mathrm{s}$, corresponding to the diffusion coefficient of a molecule with a 20 kDalton mass (*i.e.* the mass of IL-6) in the cytoplasm environment. If the molecule reaches a cell, it is internalized (depletion) and stops diffusing, whereas the cells continue to release cytokines. Figure 9 shows preliminary results of simulations (with a production rate of 0.16 cytokines/(s*cell)), compared with experimental results.

3˙4. *Effects on lipids and oxidative metabolism; intercellular signalling mechanisms investigated by MRS*. – The development of non-invasive methods to detect the effects of radiation in whole intact cells *in vitro* can provide information on new targets for radiation responses including molecules different from DNA, either in cells directly hit by radiation or in cells with damage induced by the so-called "bystander effect". With this respect, the identification of new targets [23] is important to monitor radiation responses that may be differently expressed in different tumors and in normal tissues as well. Cell metabolism may be studied by means of high-resolution Magnetic Resonance Spectroscopy (MRS) in living cells in culture. In selected pathologies, this technique is used *in vivo* for diagnostic purposes, after evidence-based observations on biomarker signals in multicentric studies [24, 25]. A large area of use of MRS in clinics is also dedicated to *ex vivo* analysis to provide information of prognostic value during management of cancer patients [26, 27]. Much work is therefore dedicated to MRS studies on intact

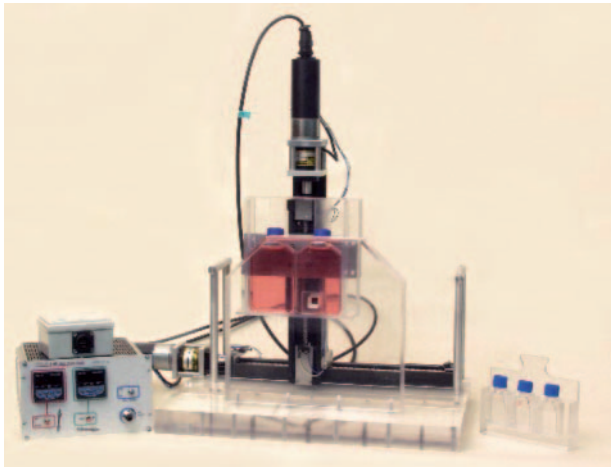

Fig. 10. – Flask holder and beam collimator. Cell flasks are inserted as shown (pink flasks) exposing sequentially regions of a square hole in the plexiglass screen (thickness 3 cm). Dimensions of the square hole match proton beam diameter in the region of 99% homogeneity. Displacement of the flasks in the (x, y)-plane, performed with two independent steppers, is affected by less than 0.05 mm error.

cells *in vitro* aiming at obtaining a better picture of cell metabolism and identification of spectroscopic markers associated to a selected biological outcome, following treatments with chemical and/or or physical agents [28]. Some signals, detectable *in vivo*, were found to be related to selected biological outcomes when cell growth was modified either by chemicals causing cell death or by treatments designed to affect cell proliferation and differentiation. The availability of new MRS instruments operating at very high fields and/or better equipments such as cryoprobes with very high sensitivity and spectral resolution allows to acquire MR spectra from very small volumes (*e.g.*, in microprobes 10–20 μl), compatible with biopsy samples.

In this work, two sets of cells with different radio-resistance were used. Initially, cells from cancer of human cervix, HeLa, were compared to cells from breast cancer, MCF-7, the latter being more resistant to irradiation by gamma-rays [29]. In a second phase of the study, A172 and T98G cells from human glioma were studied, the latter being more radio-resistant. Cells were irradiated with gamma-rays (Co-60) and with 62 MeV proton beams at the INFN-LNS. Cells were routinely irradiated in the culture flask to avoid metabolism perturbation during cell growth. For irradiation it was necessary to build an apparatus acting as a proton beam collimation and sample holder (fig. 10). The apparatus exposed different sections of the culture flasks moving the sample holder in a sequential, operator-controlled, fashion on a plane orthogonal to the beam, to expose the entire cell-covered surface.

Apoptosis was quantified along with cell killing and cell cycle arrest, to characterize biological effects and to find a correlation with the spectroscopic observations. In HeLa cells, maximum apoptosis was found after 24 hours from gamma-irradiated samples that underwent significant apoptotic death, while in MCF 7 cells the percentage of apoptotic cells was not significant. In MCF-7 cells, apoptosis after irradiation was induced only after buthionine sulfoximine (BSO) treatment. This treatment induced GSH depletion by inhibition of GSH synthesis: MCF-7 cells, deprived of the antioxidant protection,

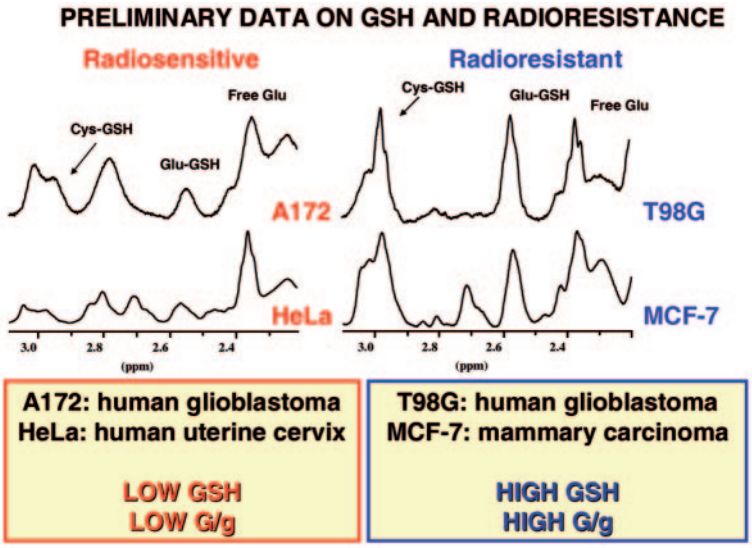

Fig. 11. – High-resolution 1 H MR spectra at 600 MHz from glutathione region cell samples. Spectra were acquired by means of a Bruker 1 mm microprobe at 289 K, under solvent suppression conditions. G = glutamate in GSH, g = free glutamate.

were then able to undergo apoptosis. As already observed in HeLa cells, the maximum percentage of apoptotic cells was found at 24 hours after irradiation. Time-kinetics of apoptosis was found to be affected by LET in both cell lines: irradiation with proton beams shifted the maximum percentage of apoptotic cells to 48 hours.

Among the visible peaks in MR spectra two sets of signals were analyzed, due to their possible detection also from *in vivo* MRS. One set of signals is from reduced glutathione (GSH), due to the important role of this molecule to act as detoxifying agent. At present, quantification of GSH concentration may usually be performed by means of destructive analytical methods. In MR spectra this molecule shows narrow signals, the most prominent being that from glutamate, which was used for relative quantification. After irradiation by gamma-rays and proton beams, GSH signals show intensity changes that indicate consumption by detoxification reactions and increased activity of the γ-glutamyl cysteine synthetase. Relative GSH concentration, as measured by MRS, was found consistent with radio-sensitivity (fig. 11). Low GSH concentration, either naturally occurring, as in HeLa and A172 cells, or artificially produced, by treatment with BSO, was correlated with relevant apoptosis.

The second set of MRS signals studied was related to the structures known as mobile lipids (ML), mostly arising from the neutral lipids, triglycerides, present in the spectra of tumour cells. The analysis of the spectra from both cell lines showed different spectral behaviour after irradiation. The intensities of signals from neutral lipids were measured in irradiated cell samples with respect to the corresponding non-irradiated controls. Spectra from perchloric acid extracts and total extracted lipids were also run. According to previously reported data [30], intensity modulation of lipid signals accompanies cell growth: intensity variation was then monitored after different time intervals from irradiation. A common feature of the two cell lines was a marked decrease of lipid signals after seeding. In this region irradiation did not induce relevant changes. Subsequently,

HeLa cells, undergoing extensive apoptosis, displayed lower lipid intensity in irradiated *vs.* control samples, while MCF-7 cells, which underwent very little apoptosis, showed more intense lipid signals in irradiated samples. This behaviour was therefore not related to the occurrence of apoptosis, as suggested by other authors [31]. The extent of the phenomenon was dose and LET dependent. Finally, in order to provide possible application of MRS to the study of bystander effect, some preliminary results were obtained on sampled medium of irradiated cells in comparison with medium from controls. It has been suggested that cell communication might not be limited to soluble agonists, but that various types of vesicles also participate in the process [32]. The phenomenon, detected in different cell systems by many authors, was also studied by MRS [33]. Preliminary data point to differences on relative intensities of lipid-related signals in cell medium before and after irradiation. This finding is in agreement with those from other authors [34], who demonstrated the production of exosomes into the medium after radiation-induced DNA damage, suggesting that these vesicles can communicate with adjacent cells. Work is in progress to clarify this point.

4. – Conclusions and future developments

In this paper we presented the outcomes of a large collaborative effort (carried out within the INFN project "EPICA" and in part within the European projects "RISC-RAD" and "NOTE" and the ASI project MoMa-COUNT) devoted to the characterization and quantification of the induction of DNA-targeted and non-DNA-targeted molecular and cellular biological endpoints following irradiation of normal and cancer human cells with different charged particles, gamma-rays acting as the reference radiation. The main aim of this work consisted of reaching a better understanding of the mechanisms governing the physical and biophysical pathways leading from the initial energy deposition by radiation in matter to the induction of observable radiobiological damage, with great focus on the role played by radiation quality (*i.e.* particle type and energy, LET). The induction of DNA DSB was characterized experimentally and theoretically within different fragment-size ranges. Our results highlight the effectiveness of high-LET radiation at inducing small fragments, which reflect the clustering properties of radiation track structure and are correlated with the induction of severe damage. Such damage is hard to repair and can thus lead, for example, to chromosome aberrations (CAs). This was confirmed by a model of CA induction based on the assumption that only severe DNA breaks can lead to aberrations.

Concerning non-DNA-targeted damage, we quantified the time-dependent induction of medium-mediated DNA damage in bystander cells, which showed a significant increase of H2AX phosphorilation foci after 1 and 2 hours of co-culture with irradiated cells. To investigate the mechanisms underlying medium-mediated bystander damage, which are thought to be based on cell-to-cell communication via signalling molecules such as cytokines, we characterized the time- and dose-dependence of cytokine (*e.g.*, IL-6) concentration in the culture medium of sham-irradiated and irradiated cells. We reported an initial increase followed by a saturation-like pattern at several hours after irradiation. The release, diffusion and internalization of cytokines were simulated by a theoretical model and a MC code which assume a Brownian-like diffusion followed by cytokine depletion. This showed a good agreement with experimental data on sham-irradiated cells. Non-DNA-targeted effects were further characterized by MRS-based investigation of the radiation effects on lipids and oxidative metabolism. The latter are particularly relevant considering that they may be differently expressed in tumors and normal tissues.

We plan to focus future work on heavy ions such as carbon, which is of great importance because of its use in cancer therapy, and on non-DNA-targeted effects, both in terms of the mechanisms underlying phenomena like bystander effects, and in terms of the modulation of molecular signaling by radiation.

* * *

This work was partially supported by INFN-CSN5 (EPICA experiment), EU ("RISC-RAD" project, Contract no. FI6R-CT-2003-508842, and "NOTE" project, Contract no. FI6R-036465) and ASI (Italian Space Agency, "Mo-Ma/COUNT" project). We would like to thank the INFN-LNS, particularly G. Cuttone and all the staff of the laboratory.

REFERENCES

[1] Goodhead D. T., *Int. J. Radiat. Biol.*, **65** (1994) 7.
[2] Friedland W., Jacob P., Paretzke H. G., Ottolenghi A., Ballarini F. and Liotta M., *Radiat. Prot. Dosim.*, **122** (2006) 116.
[3] Holley W. R. and Chatterjee A., *Radiat. Res.*, **145** (2006) 188.
[4] Rydberg B., Holley W. R., Mian I. S. and Chatterjee A., *J. Mol. Biol.*, **284** (2006) 71.
[5] Belli M., Cherubini R., Dalla Vecchia M., Dini V., Esposito G., Moschini G., Sapora O., Simone G. and Tabocchini M. A., *Int. J. Radiat. Biol.*, **78** (2006) 475.
[6] Löbrich M., Cooper P. K. and Rydberg B., *Int. J. Radiat. Biol.*, **70** (1996) 493.
[7] Dini V., Antonelli F., Belli M., Campa A., Esposito G., Simone G., Sorrentino E. and Tabocchini M. A., *Radiat. Res.*, **164** (2005) 577.
[8] Belli M., Campa A., Dini V., Esposito G., Furusawa Y., Simone G., Sorrentino E. and Tabocchini M. A., *Radiat. Res.*, **165** (2006) 713.
[9] Rogakou E. P., Boon C., Redon C. and Bonner W. B., *J. Cell Biol.*, **146** (1999) 905.
[10] Taneja N., Davis M., Choy J. S., Beckett M. A., Singh R., Kron S. J. and Weichselbaum R. R., *J. Biol. Chem.*, **279** (2004) 2273.
[11] Campa A., Ballarini F., Belli M., Cherubini R., Dini V., Esposito G., Friedland W., Gerardi S., Molinelli S., Ottolenghi A., Paretzke H., Simone G. and Tabocchini M. A., *Int. J. Radiat. Biol.*, **81** (2005) 841.
[12] Friedland W., Ballarini F., Cremer C., Kreth G., Ottolenghi A. and Paretzke H. G., *Radiat. Environ. Biophys.*, **47** (2008) 49.
[13] Campa A., Esposito G., Belli M., Simone G. and Tabocchini M. A., *Int. J. Radiat. Biol.*, **80** (2004) 229.
[14] Lea D. E., *Actions of Radiations on Living Cells* (Cambridge University Press, Cambridge, UK) 1946.
[15] Ballarini F., Merzagora M., Monforti F., Durante M., Gialanella G., Grossi G., Pugliese M. and Ottolenghi A., *Int. J. Radiat. Biol.*, **75** (1999) 35.
[16] Ballarini F. and Ottolenghi A., *Adv. Space Res.*, **31** (2003) 1557.
[17] Ballarini F. and Ottolenghi A., *Radiat. Environ. Biophys.*, **43** (2004) 165.
[18] Ballarini F. and Ottolenghi A., *Radiat. Res.*, **164** (2005) 567.
[19] Ballarini F., Biaggi M. and Ottolenghi A., *Radiat. Prot. Dosim.*, **99** (2002) 175.
[20] Ballarini F., Alloni D., Facoetti A., Mairani A., Nano R. and Ottolenghi A., *Adv. Space Res.*, **40** (2007) 1392.
[21] George K., Durante M., Willingham V., Wu H., Yang T. and Cucinotta F. A., *Radiat. Res.*, **160** (2003) 425.
[22] Azzam E. I., De Toledo S. M. and Little J. B., *Proc. Natl. Acad. Sci. USA*, **98** (2001) 473.
[23] Overgaard J. and Baumann M., *Radiotherapy and Oncology*, **83** (2007) 217.
[24] Cheng L. L., Burns M. A., Taylor J. L., He W., Halpern E. F., Mcdougal W. S. and Wu Chin-Lee, *Cancer Res.*, **65** (2005) 3030.

[25] Katz-Brull R., Lavin P. T. and Lenkinski R. E., *J. Natl. Cancer Inst.*, **94** (2002) 1197.
[26] Lindskog M., Spenger C., Jarvet J., Graslund A. and Kogner P., *J. Natl. Cancer Inst.*, **96** (2004) 1457.
[27] Sorensen G., *J. Clin. Oncol.*, **24** (2006) 3274.
[28] Evelhoch J., Garwood M., Vigneron D., Knopp M., Sullivan D., Menkens A., Clarke L. and Liu, *Cancer Res.*, **65** (2005) 7041.
[29] Rosi A., Grande S., Luciani A. M., Palma A., Giovannini C., Guidoni L., Sapora O. and Viti V., *Radiat. Res.*, **167** (2007) 268.
[30] Rosi A., Luciani A. M., Matarrese P., Arancia G., Viti V. and Guidoni L., *Magn. Res. Med.*, **42** (1999) 248.
[31] Hakumaki J. M. and Liimatainen T., *Eur. J. Radiol.*, **56** (2005) 143.
[32] Denzer K., Kleijmeer M. J., Heijnen H. F., Stoorvogel W. and Geuze H. J., *J. Cell Sci.*, **113** (2000) 3365.
[33] Laulagnier K., Motta C., Hamdi S., Roy S., Fauvelle F., Ois Pageaux J. F., Kobayashi T., Salles J. P., Perret B., Bonnerot C. and Record M., *Biochem. J.*, **380** (2004) 161.
[34] Yu X., Harris S. and Levine A., *Cancer Res.*, **66** (2006) 4795.